

1 Shear Modulus of Cylindrical CFRP Tendons

2 Exposed to Moisture

3 Eleni Toumpanaki¹, Janet M. Lees², Giovanni P. Terrasi³

4 Abstract

5 Two groups of cylindrical CFRP tendons were exposed in distilled water at 23°C and 60
6 °C to study the diffusion mechanisms and the effect of moisture uptake on the tendon
7 shear modulus. The two tendon groups had different manufacturing processes, so DMA
8 tests and optical microscopy were used to help characterise the materials. Mass uptake
9 readings of tendon samples were recorded and the uptake generally agreed with Fickian
10 predictions. To study the time-dependent changes in the matrix stiffness due to exposure,
11 torsion tests within the elastic range of loading were conducted. The tendon shear modulus
12 was then derived from the torque versus twist plots. For both groups of tendons the
13 measured shear modulus decreased due to exposure in water. A long-term shear modulus
14 prediction model was developed to relate the tendon torsional shear stiffness and the
15 moisture concentration and the results appeared to agree well with the experimental
16 findings.

17
18 **Author Keywords:** Carbon fiber reinforced polymer, Durability, Prediction model

¹Ph.D. Candidate, Department of Engineering, University of Cambridge, Trumpington Street, Cambridge, UK, CB2 1PZ, Tel: +44(0)12233 32758, e-mail: et343@cam.ac.uk (corresponding author)

²Reader in Civil Engineering, Department of Engineering, University of Cambridge, Trumpington Street, Cambridge, UK, CB2 1PZ, e-mail: jml2@eng.cam.ac.uk

³Head, Laboratory for Mechanical Systems Engineering, Swiss Federal Laboratories for Materials Science and Technology (EMPA), Überlandstrasse 129, 8600 Dübendorf, Switzerland, e-mail: giovanni.terrasi@empa.ch

19 **Introduction**

20 Recent high-profile incidents of the corrosion of steel reinforcement in prestressed
21 concrete bridge structures, e.g. the Mid Bay Bridge in Florida (Hartt and Venugopalan
22 2002) and Hammersmith Flyover Bridge in London (Lynch 2012), have exemplified the
23 extensive disruption and costs associated with steel corrosion. The use of fibre reinforced
24 polymer (FRP) tendons as internal concrete reinforcement is a proactive means to avoid
25 chemical corrosion. Despite their high initial cost, FRP tendons can be effective in terms
26 of the whole life costing of a structure and the full strain capacity can be exploited if the
27 tendons are prestressed (Burgoyne and Balafas 2007). However, a lack of confidence in
28 the adoption of new structural materials has limited the wider field applications of FRPs.
29 Moreover, the long term durability of FRPs in wet environments remains an area of active
30 research. It is important to ensure that FRP tendons are not adversely affected due to
31 moisture absorption in the resin matrix material.

32
33 To date, design guidelines and codes for concrete reinforced with carbon FRP (CFRP)
34 have proposed strength reduction factors for environmental exposure, but due to the
35 complexities of the interactions there can be a lack of a firm experimental or analytical
36 basis to support these recommendations (Huang and Aboutaha 2010). Furthermore, the
37 strength reduction factors tend to relate to fibre dominated properties, such as tensile
38 strength (ACI 2006), but do not necessarily reflect matrix dominated properties, such as
39 the bond performance, shear strength, dowel strength and creep, all of which can be
40 degraded from exposure in wet environments. Another factor not explicitly considered by
41 standards is the manufacturing process of the CFRP tendons and in particular the curing
42 (Krishna et al. 2010).

43

44 **Manufacturing process in CFRP tendons**

45 The most suitable manufacturing process for cylindrical FRP bars used as prestressing
46 tendons is the pultrusion method. Pultrusion offers a high speed of production for constant
47 circular cross sections with high fibre volume fractions. The resulting bars have a high
48 stiffness through the alignment of unidirectional fibres (Mayer 1996). The final quality of
49 the CFRP tendons is regulated by a low void percentage and a high crosslinking density of
50 the epoxy matrix.

51

52 The die length and temperature, the pull out speed and the heat power input influence both
53 the presence and percentage of voids in pultruded FRPs (Li et al. 2002; Lam et al. 2003).

54 The fibre sizing, coupling agent and resin viscosity also play a role (Kelly 1989). The

55 effect of the void content has been mainly studied in aerospace engineering, since

56 increased porosity has been reported in laminate structures. This most commonly occurs in
57 the resin rich interface layers as a result of the lay-up manufacturing process. Voids have a

58 greater effect on the interlaminar shear (ILSS) and flexural strength than on the tensile

59 modulus and strength (Olivier et al. 1995; Liu et al. 2006). This is because pores replace

60 the matrix material and develop preferentially in the fibre-matrix interface. Even for the

61 same absolute void percentage large variations in performance have been reported due to a

62 dependency on the width to length aspect ratio of the voids (Huang and Talreja 2005; Zhu

63 et al. 2009). Hancox (1977) reported a 70% decrease in shear modulus and strength of wet

64 moulded CFRP rods with a 5% void content and observed that interconnected void regions

65 enable the shear crack paths to initiate and develop. Zhu et al. (2009) recorded a drop of up

66 to 16% in the ILSS of carbon/epoxy laminates with 8% porosity relative to laminates with

67 0.2% porosity.

68

69 The curing temperature and curing time in the manufacturing process controls the degree
70 of molecular crosslinking in a resin matrix and consequently influences the chemical
71 stability and mechanical performance on the macroscale. The polymerisation of epoxy
72 groups is the result of three principal curing reactions. The first curing reaction is between
73 an epoxide group and the primary amine group of the curing agent. The second reaction
74 has a lower rate and a second curing run is often required for the full conversion of the
75 secondary amines (Vanlandingham et al. 1999a). The etherification of the remaining
76 unreacted and reacted epoxy groups is the final stage of the curing process and takes place
77 only at high temperatures and longer times (Vanlandingham et al. 1999a) or in the
78 presence of catalysts (Wu 1992) . In practice the experimental detection of the degree of
79 crosslinking in epoxies is difficult and consequently the molecular structure and
80 mechanical properties cannot be directly related. The most commonly used methods to
81 infer the crosslinking density are by determining the glass transition temperature (T_g)
82 values using Dynamic Mechanical Analysis (DMA) (e.g. Vanlandingham et al. 1999a) and
83 Differential Scanning Calorimetry (DSC) (e.g. Wu 1992) . A higher crosslinking density is
84 believed to result in a higher T_g value (Wu 1992; Vanlandingham et al. 1999a).

85

86 **Exposure to moisture**

87 In humid environments, the matrix component of a CFRP tendon is the main source of
88 degradation, since carbon fibres are generally considered to be impermeable due to their
89 highly aligned and crystalline structure. The moisture diffusion process in epoxies is
90 governed by two factors. The first is the availability of molecular sized holes (free volume)
91 which is inherently dependent on the crosslinking density (Diamant et al. 1981;
92 Vanlandingham et al. 1999b) and hence on the hardener type and extent of cure (Diamant
93 et al. 1981; Wright 1981). This process is reversible upon drying. The second factor is the

94 hydrogen bonding of the water molecules in the sorption sites in the polymer such as the
95 hydroxyl groups (bound molecules). This process is irreversible and leads to the swelling
96 of the epoxy matrix material (Adamson 1980). The water uptake in epoxies is also affected
97 by a number of other parameters including the polymer polarity, unreacted amine groups,
98 and the development of a two phase structure (Diamant et al. 1981). All these factors are
99 related to the manufacturing variables, such as the stoichiometry, mixing conditions,
100 temperature, extent of cure and pressure. A decrease in the diffusivity of epoxy systems
101 (Marais et al. 2000) and the water saturation levels in CFRPs (Ankara et al. 1986) have
102 been attributed to a higher degree of cure and additional crosslinking. However, Min et al.
103 (1993) have found that additional crosslinking does not necessarily result in a lower
104 diffusivity.

105
106 Accelerated ageing can be used to obtain long-term data from short exposure times. The
107 most widely accepted method based on the Arrhenius principles is to accelerate moisture
108 uptake with the application of elevated temperatures in conjunction with exposure in
109 humid environments. It is assumed that one chemical degradation mechanism exists and
110 accelerates by elevating the temperature. However, longer exposure times and longer
111 exposure temperatures may cause hydrolysis resulting in mass loss. In general, CFRP
112 tendons exhibit a good chemical resistance against hydrolysis (chain scission) due to the
113 stability of the epoxy resin and carbon fibres when subjected to wet environments.

114 Nevertheless, hydrolysis has been observed in epoxy matrices exposed in distilled water at
115 high temperatures near the glass transition temperature of the exposed sample (Xiao and
116 Shanahan 1997). Therefore, the temperature applied should be much lower than the T_g
117 value of the unexposed epoxy to avoid additional degradation mechanisms that are not
118 representative. However, moisture absorption decreases the T_g of the epoxies and hence a

119 safe threshold should be defined. Dolan et al. (2008) suggested that an elevated exposure
120 temperature should be at least 15°C lower than the T_g value. However, a reduction in T_g of
121 up to 30°C has been reported in a CFRP laminate exposed at 95% RH and 50°C for 1.7%
122 moisture uptake and with a reference T_g value of 135°C (Birger et al. 1989). Furthermore,
123 Robert et al. (2010) observed additional degradation mechanisms in GFRP bars immersed
124 in distilled water at 80°C, even though the T_g of an unexposed specimen was 96°C.
125 According to ACI (2006), 60°C is recommended as an accelerated ageing temperature for
126 structural FRP materials.

127

128 **Effect of moisture on strength and stiffness**

129 A common test method to assess the long-term durability of matrix dominated properties
130 in FRPs is the short beam test method. This method can provide insight into both the
131 stiffness and strength implications of moisture exposure. In the context of a matrix
132 strength assessment, the test is more directly applicable to laminate structures, where the
133 failure takes place mostly between laminas and so the interlaminar shear stress (ILSS) can
134 be derived. In durability tests on unidirectional carbon/epoxy laminates manufactured
135 with a wet lay-up method, Abanilla et al. (2006) reported a 33.4% reduction in
136 interlaminar shear strength after 100 weeks of exposure in alkaline solution and a 20%
137 reduction in interlaminar shear modulus after 100 weeks of exposure in deionised water at
138 23°C. Interlaminar shear strength reductions in CFRP rods of 14-35% have been reported
139 after exposure in alkali solution at 60°C for 42 days (Micelli and Nanni 2001). Scott and
140 Lees (2012) conducted short beam shear tests on CFRP tendons that had been immersed in
141 either water (W), salt water (SW) or concrete pore solution (CPS) for roughly 1.5 years at
142 60 °C. For specimens without axial stress loaded transversely with flat plates, the ultimate
143 shear load of the SW and W specimens did not differ significantly from the unexposed

144 control samples but a 7% loss of strength was noted after CPS exposure. The average
145 measured stiffnesses of the exposed tendons were less than the unexposed samples and, for
146 example, the load versus deflection slope for the water-exposed samples was around 30%
147 lower at small displacements. Transverse shear tests on CFRP tendons using rounded
148 plates were also conducted. However, it was postulated that the inference of the matrix
149 strength from the peak load may result in misleading conclusions since in these tests the
150 failure process can shift from a matrix-dominated to fiber-dominated mechanism (Scott
151 and Lees, 2012). Such fiber-dominated effects also have ramifications for the measured
152 matrix stiffness. Scott and Lees (2012) noted three stages of behaviour from the rounded
153 plate load deflection results. The first stage at small displacements was felt to be the most
154 representative of the matrix stiffness. The tendons then delaminated which led to a second
155 phase of behavior associated with further delamination and an increase in displacement
156 under constant load. A final phase, after large displacements, was characterized by a stiffer
157 response associated with fiber-stiffening mechanisms. In short beam tests on GFRP rods,
158 Chen et al. (2007a) observed a lower slope in the load versus deflection plots for
159 deflections up to 0.5 mm and attributed this to the low matrix strength and stiffness. But
160 the slope then increased with increasing load up to failure.

161

162 **Torsion testing**

163 To study changes in matrix stiffness due to moisture exposure and to mitigate the fibre
164 stiffening mechanisms prevalent in short beam shear tests, the current work investigates
165 the testing of CFRP rods in torsion. In a torsion test, the shear modulus of an FRP rod, in a
166 plane perpendicular to the fibre direction, can be measured while minimising stress
167 concentrations and normal bending stresses. Studies on the torsional mechanical behaviour
168 of CFRP rods (Hancox 1972; Hiermer et al. 1998) and laminates (Ogasawara et al. 2007)

169 have been carried out, but have primarily focused on the elastic-plastic behaviour and the
170 ultimate strength properties. For cylindrical tendons, the stiffness of the epoxy matrix can
171 be derived from the torsional shear modulus values and at small rotations fibre stiffening
172 effects are minimised. A further advantage is that, after exposure, the moisture uptake
173 occurs first in the outer perimeters of the CFRP cross-section. In a torsion test, it is the
174 outer perimeter where the maximum torsional shear stresses act and contribute most to the
175 shear stiffness. Therefore, any degradation of these regions can be observed after relatively
176 short exposure times. CFRP tendons, produced using two different manufacturing
177 methods, are studied. To characterise the tendon moisture uptake properties, the diffusion
178 behaviour is studied with short tendon samples immersed in water at 23°C and 60°C.
179 CFRP tendons are tested elastically in torsion after different exposure times to investigate
180 the relationship between the moisture uptake and shear modulus degradation. A model
181 relating the radial diffusion to the change in shear modulus is developed to predict the
182 shear modulus degradation with time.

183

184 **Experimental Program**

185 **Materials**

186 The CFRP tendons used in this research are categorised into two groups C and D, based on
187 their manufacturing details. Both groups of tendons had the same Bakelite EPR 4434
188 epoxy and EPH 943 hardener, Tenax UTS 5631 fibres and fibre volume fraction, $V_f=64\%$.
189 However, the nominal tendon diameters differed and were 4.2 mm and 5.4 mm for groups
190 C and D respectively. These values refer to the nominal diameter of the core tendon as
191 provided by the manufacturer and were adopted in the following calculations. The core
192 diameters of both groups C and D tendons were also measured with a micrometer and

193 found to be $\Phi=4.15 \pm 0.06$ mm and $\Phi=5.44 \pm 0.014$ mm respectively. The group C tendons
194 were manufactured specifically for research purposes and were uncoated. In contrast, the
195 group D specimens were commercial products and so had a sand coating layer to improve
196 the bond between the tendon and concrete. This means that there was an additional in-line
197 production step during pultrusion, where an additional epoxy layer was applied, sand
198 particles were sprayed and further curing followed. For this experimental series the sand
199 coating layer was gently scraped off with a sharpened blade from the group D CFRP
200 tendons. The exact details of the cure cycle are confidential but during the curing process
201 the group C and D tendons were heated to a maximum temperature of 195°C.

202

203 **Material characterization: Optical Microscopy and DMA tests**

204 To verify the quality of the manufacture, the fibre size and the fibre-matrix interface,
205 samples were studied using a Leica DMLM Optical Microscope (Leica Microsystems,
206 Germany). Unexposed tendon samples were cut with a Dremel 398 tool (Dremel Europe,
207 UK) and cast into a resin matrix (Acri-kleer cold mounting). The samples were later
208 polished with P800 (22 μm) and P400 (5 μm) abrasive silicon paper.

209

210 Dynamical Mechanical Analysis (DMA) tests were conducted to measure the T_g values of
211 the CFRP tendons and to infer the crosslinking density of the epoxy, since these two
212 properties are felt to be interrelated (Min et al. 1993; Vanlandingham et al. 1999a). Two
213 samples from group C (C_1 & C_2) and one sample from group D (D_1) were tested. The
214 number of the tested specimens is limited and not sufficient for a full statistical analysis.
215 Nonetheless, the DMA results can help to identify fundamental differences between the
216 two tendon groups. The specimens were 40 mm long and were machined to square

217 sections of 3.10mm × 3.10 mm for group C and 3.60 mm × 3.60 mm for group D. The
218 dimensions varied at most by 1% along the length of the specimens. All specimens were
219 preconditioned at 23°C ± 2°C and RH = 50% ± 5 % for at least 7 days before testing in a 3
220 point bending mode. The ramp rate was 2°C/min, the frequency was fixed at 10 Hz, the
221 temperature ranged from 23°C – 210°C and strain amplitude of 0.02 mm was applied. The
222 T_g values were measured from the peak of the $\tan\delta$ plot.

223

224 **Exposure and moisture absorption**

225 A number of 100 mm tendon samples were immersed for moisture absorption tests, where
226 the mass weight was recorded at different times. Five 100mm length CFRP samples from
227 both groups C and D were fully immersed in distilled water in separate polypropylene
228 containers and were stored in the lab at room temperature (23°C). In addition, four
229 immersed samples from group C and two samples from group D were stored in the oven at
230 60°C to accelerate the ageing process. The 60°C exposure conditions are well below the
231 measured T_g values of the epoxy used (see next section) and so this temperature was
232 unlikely to invoke unrepresentative degradation mechanisms. The mass uptake in the 100
233 mm samples was regularly recorded using an Oertling R20 (Oertling Ltd, UK) analogue
234 balance machine with a 0.0001 g resolution. Before each measurement the specimens were
235 blotted dry with a tissue paper and left at room temperature for 5 min. The average of three
236 separate mass readings was recorded as the mass weight at a given time.

237

238 **Torsion rig and torsion testing procedure**

239 The torsion rig set-up is shown in Figure 1a. The torsion tests were carried out according
240 to ASTM E143-02. One end of a 300 mm long tendon is gripped in a three jaw chuck,

241 while the other end is free to twist. At the right hand support, a fixed bearing enables axial
242 movement through a long recess which extends beyond the length required to support the
243 tendon (Figure 1b). A perpendicular lever arm is attached to the tendon using the clamp
244 shown in Figure 1c. A rubber layer is inserted between the tendon and the clamp to
245 enhance the friction and avoid slipping. A spirit level fixed on the lever arm ensures the
246 tendon is correctly aligned before testing. Loading weights of 50 g are applied to the lever
247 arm through a wire. The torque was calculated as the load multiplied by the lever arm
248 (162 mm) but was corrected for the change in the angle of the lever arm. Inclinometers
249 with a range -15° to 15° and with a 0.0006° resolution measured the rotation of the
250 specimens. The inclinometers were calibrated before every torsion test and the resulting
251 calibration factors were validated against a specified nominal range. Each inclinometer is
252 attached through a mounting plate to a hexagonal section at the midpoint of the
253 inclinometer that is secured with three bolts to the tendon. The relative twist was
254 calculated at each loading step as the difference between the readings of two inclinometers
255 over a distance of 105 mm. To investigate the accuracy of the experimental set up, initial
256 torsion tests were carried out on a steel rod with a diameter of 4.76 mm. The
257 experimentally measured modulus was found to deviate from the nominal shear modulus
258 of steel by 1.6-4%. To assess the inherent material variability between CFRP tendons,
259 three unexposed specimens from group C, derived from the same length of the tendon roll,
260 were tested and the shear modulus values were found to vary by 2.5%.

261

262 **Experimental series**

263 The experimental programme consisting of two test series is summarised in Table 1. The
264 main experimental variables were: specimen type (group C or D), drying time, exposure
265 time, exposure temperature (23°C and/or 60°C), and the effects of repeated testing.

266

267 All the specimens had been previously stored in lab conditions and dried in an oven at
268 60°C prior to exposure. In series I, the specimens were dried for 2 years. However, after
269 204 days a mass loss of up to 0.54% for groups C and 0.58% for group D was recorded
270 and thereafter no further mass loss was observed. At the end of the drying period, no
271 cracks or discolouration were visually observed, so we assume no thermo-oxidative ageing
272 effects took place. For series II, the specimens were dried for only 4 months but the mass
273 was found to differ by about 0.10% from series I. In the following discussion, the drying
274 period is not taken as a differentiator.

275

276 Control specimens (C-II-3 and D-I-7) were used to measure the baseline dry shear
277 modulus. For the exposed specimens, a 200 mm central region of the 300 mm long sample
278 was immersed in distilled water. This was to protect the region that will be clamped in the
279 torsion test and avoid a premature failure since CFRPs are susceptible to lateral
280 compression when exposed to humid environments. The majority of the specimens were
281 exposed continuously to either 23°C or 60°C. The exceptions were specimens D-I-9 and
282 C-I-8 which were moved after exposure for 141 days at 23°C to an oven at 60°C under
283 similar immersion conditions. This was done to further investigate the equivalency of the
284 total moisture uptake regardless of exposure temperature.

285

286 For all the exposed specimens, the same tendon specimen was tested at two or more
287 different time intervals. But there was a concern that if microcracking occurred during a
288 torsion test at a given time interval, this could then precipitate additional moisture uptake
289 such that a greater stiffness degradation might be observed at the next time interval. A
290 range of comparable specimens were therefore tested such that the second time of testing

291 coincided with the first testing of another specimen at the same exposure time (e.g. C-II-9
292 to C-II-12 and C-II-4 to C-II-7). Hence, if the shear moduli differed beyond the
293 experimental error range allowing for a degree of material variability, this would indicate
294 that microcracking could play a role. In addition, since the exposure time at first testing
295 also varied, any dependency of the microcracking on moisture uptake could also be
296 ascertained.

297

298 Specimens C-I-6 and D-I-6 were the first specimens to be tested and used a torsion test set-
299 up with a slightly different right hand support condition. C-I-6 also used a flat plate
300 clamping system which was subsequently changed since there were signs of damage in the
301 clamping region near the exposed area after testing at 112 days. The clamping system used
302 in all the other tests had a curved profile (see Figure 1c) that provided a more uniform
303 radial stress distribution.

304

305 The aim was to ensure that under the applied torsional stress, the tendons remained in the
306 elastic range. Based on research work by Hancox (1972) on unidirectional CFRP bars and
307 Ogasawara et al. (2007) who studied unidirectional CFRP laminates, the maximum values
308 of torsion shear stresses τ in the elastic range were 24 and 32 MPa respectively. Failure
309 trial tests on group C specimens showed a linear relationship up to approximately 31 MPa.
310 In the experimental procedure, group C specimens were loaded up to maximum total
311 weight of 200 g whereas a maximum of 250 g was used for group D. The theoretical
312 maximum values of τ at the maximum loading are 21 MPa for group C and 13 MPa for
313 group D so should remain in the elastic range.

314

315 **Results and Discussion**

316 **Optical Microscopy**

317 Figure 2a shows a section of a group C sample at a magnification of 1000 μm . The
318 percentage of voids is significant and extends to long interconnected regions within the
319 resin matrix with a length up to 500 μm and width in the order of 20-30 μm (Figure 2b).
320 Furthermore, a region of different morphology is observed that is characterised by a dense
321 distribution of smaller fibre sizes (Figure 2c, 2d). Similar findings have also been reported
322 in commercially available GFRP tendons by Davalos et al. (2008). Optical microscope
323 pictures for Group D samples reveal a solid matrix distribution and a uniform size of fibres
324 as shown in Figures 3a & b. The only abnormalities are small areas of different ‘glassy’
325 morphology (Figures 3 c and d) that have also been observed in group C. This is more
326 pronounced in Figure 3d, where a dark field is applied for comparison. This might be
327 indicative of a two-phase morphology with phases of lower crosslinked structure in the
328 order of 10-20 μm . Soft phases of lower crosslinked structure have been reported by
329 Vanlandingham et al. (1999a) in Atomic Force Microscope pictures of stoichiometric
330 compositions of high crosslink density Epoxy EPON-828 and PACM 20.

331

332 **DMA tests**

333 Figure 4 illustrates the storage modulus E' and $\tan\delta$ values with respect to temperature.
334 The DMA tests yielded $T_{g-\tan\delta}=163$ and 170°C for the two group C samples and
335 $T_{g-\tan\delta}=147^\circ\text{C}$ for the group D specimen. The higher group C T_g values would suggest a
336 higher crosslink density. This is contradictory to what was expected, since group D was
337 additionally heated during production when the sand coating was applied. Although an
338 increase in T_g values due to post-curing has been reported elsewhere (Wu 1992) this is not

339 observed here and the group D specimens have a T_g which is 15°C lower than group C.
340 However, group D has a higher absolute peak $\tan\delta$ value and a narrow α -relaxation that is
341 indicative of a higher crosslink density (Meyer et al. 1995). In group C the $\tan\delta$ vs
342 temperature plot has a wider α -relaxation that is shifted to higher temperatures resulting in
343 higher T_g values. Meyer et al. (1995) observed a slight increase in width of α - relaxation in
344 connection with lower $T_{g-\tan\delta}$ values in epoxy rich samples that exhibited lower crosslink
345 density. Furthermore, the sample C1 exhibits a small relaxation phase in the range of
346 60°C-80°C. This phase is denoted as the ω -relaxation phase for the purposes of this paper.
347 A ω -relaxation phase at lower temperature ranges has been reported elsewhere (Meyer et
348 al. 1995; Cavaille et al. 1987) and attributed to a lower crosslink density structure with two
349 phase morphologies in epoxy systems. It is not yet possible to conclude whether this is the
350 case for group C. The relaxation phase might also be indicative of moisture evaporation
351 acting as a plasticising agent but it is not observed in group D. The presence of voids in
352 group C could affect the results, although a lower storage modulus would be expected.

353

354 **Moisture Absorption**

355 The average mass uptake readings due to exposure in distilled water at 23°C and 60°C for
356 Group C and D are illustrated in Figure 5. The mass uptake behaviour is characterised by a
357 high initial rate that decreases progressively with immersion time. For both temperatures,
358 the group C specimens exhibit a greater mass uptake than the group D specimens at a
359 given time. Both specimen groups concurrently reached the saturation point after
360 approximately 250 days at 60°C. The saturation point at 23°C cannot be clearly identified
361 for either group even after nearly 2 years of exposure and longer exposure times will be
362 required to clarify if the 23°C specimens approach the same mass at saturation, M_{sat} ,
363 measured at 60°C. Many researchers argue that M_{sat} depends only on the RH levels and

364 should be constant irrespective of the accelerated ageing temperature (Diamant et al. 1981;
365 Marais et al. 2000; Papanicolaou et al. 2006). Wright (1981) suggests a small correlation
366 between M_{sat} and temperature, whereas increased M_{sat} values at elevated temperatures have
367 been attributed to either exposure at temperatures close to the wet T_g value (Robert et al.
368 2010) or weakening of the fibre matrix interface (Davies et al. 1996).

369

370 For comparison purposes, Fickian models have been plotted on Figure 5 for each tendon
371 group and exposure temperature. Fickian diffusion is based on the principle of the random
372 motion of molecules. In long cylinders the radial diffusion governs and by integrating the
373 concentration gradient of the solution along the radius of the specimen, Fick's laws can be
374 expressed in terms of mass uptake (Crank 1975):

$$375 \quad \frac{M_t}{M_{sat}} = 1 - \sum_{n=1}^{\infty} \frac{4}{a^2 a_n^2} \exp(-Da_n^2 t) \quad (1)$$

376 where M_t is the mass uptake at time t , M_{sat} is the mass uptake at the saturation level, a is
377 the radius of the cylindrical specimen, a_n are the roots of zero Bessel function and D is the
378 diffusion coefficient.

379 The Fickian process is dependent on two inherent material variables; M_{sat} and the diffusion
380 rate D . The most common method to calculate the diffusion rate is to calculate the gradient
381 of the experimental mass uptake M_t versus \sqrt{t} plot, and substitute into the equation:

$$382 \quad \frac{M_t}{M_{sat}} = \frac{4}{\sqrt{\pi}} \left(\frac{Dt}{a^2} \right)^{1/2} \quad (2)$$

383 However, Crank (1975) noted that the simplified form of equation (1) represented by
384 equation (2) is more valid, when $M_t \leq 0.6M_{sat}$ and is not as robust for cylinders as for the
385 equivalent expression for plane sheets. Therefore, in this study an iterative process was
386 implemented to find the diffusion coefficient by using the immersion time and the

387 respective mass uptake reading M_t as input variables. One problem is that the mass at
388 saturation M_{sat} and D are interrelated and the selected value of M_{sat} at 23°C is a source of
389 uncertainty, since saturation may not yet have been reached. Adopting as M_{sat} the latest
390 mass uptake reading at 23°C ($M_{sat}=1.43\%$ and $M_{sat}=1.00\%$ for groups C and D
391 respectively after ≈ 670 days) and 60°C ($M_{sat}=2.1\%$ for group C and $M_{sat}=1.3\%$ for group
392 D after ≈ 400 days), the derived diffusion rates are $D=4.04\times 10^{-10} \pm 6.72\times 10^{-11}$ cm²/sec
393 and $D=4.18\times 10^{-10} \pm 8.15\times 10^{-11}$ cm²/sec at 23°C, and $D=1.57\times 10^{-09} \pm 5.61\times 10^{-10}$
394 cm²/sec and $D=2.18\times 10^{-09} \pm 1.63\times 10^{-10}$ cm²/sec at 60°C for groups C and D
395 respectively. If instead it is assumed that the M_{sat} values at 23°C reach the corresponding
396 saturation levels obtained at 60°C, the average diffusivities at 23°C are then
397 $D=1.38\times 10^{-10} \pm 2.40\times 10^{-11}$ cm²/sec and $D=2.16\times 10^{-10} \pm 2.16\times 10^{-11}$ cm²/sec for
398 group C and D respectively and display a lower standard deviation. These latter values will
399 be used in all subsequent calculations relating to the 23°C behaviour and the related
400 Fickian model predications are plotted in Figure 5. The Fickian model predictions agree
401 well with the experimental data. The group D specimens have a solid matrix with no voids
402 and are more likely to comply with Fick's laws assumptions. However, in spite of the high
403 void content observed in the group C optical microscopy photos, the mass uptake
404 behaviour generally agrees with the Fickian model although a small divergence between
405 the Fickian model and the experimental data can be observed for group C at 60°C for
406 exposure between 70 and 154 days. The group C experimental data has a greater standard
407 deviation when compared with Group D. Although the group C samples have higher M_{sat}
408 values, they have lower average diffusivity values. Despite the inconclusive DMA test
409 results on the additional heating effect in group D, Krishna et al. (2010) reported decreased
410 values of M_{sat} with increased post-cure (increase of curing time and temperature) for

411 glass/epoxy specimens, whereas the diffusivity values and the time of saturation point
412 were similar. The mass uptake rate in group C during the early exposure times is higher
413 than in group D and gradually drops to lower values. This behaviour might indicate the
414 synergistic effects of voids and a two phase structure, where a lower crosslink density with
415 a higher free volume dominates during the initial exposure times. Vanlandingham et al.
416 (1999b) contended that the free volume is the governing factor in the moisture absorption
417 mechanism in epoxy-amine systems. Regardless of any crosslinking, the extent of the
418 voids in group C would be expected to dominate the mass uptake behaviour.

419

420 **Torsion tests**

421 The exposed specimens were removed from solution and tested within an hour. To
422 determine the extent of evaporation between exposure and testing, trial specimens that had
423 been exposed at 23°C for 119 days were left to dry in lab conditions. After an hour, a
424 maximum mass loss of 0.0065% and 0.004% was measured for Groups C and D
425 respectively. So the influence of evaporation was not felt to be significant.

426 For each torsion experiment, three load-unload cycles were carried out. For each load
427 cycle the graph of the torque versus twist was drawn and the shear modulus was back-
428 calculated from the gradient of the linear best fit line. The shear modulus was taken as the
429 average from the three load cycles. The unloading steps were also recorded as the weights
430 were gradually removed. Figure 6 shows the load-unload curves of a dried and saturated
431 specimen from C-II series. The loading behaviour can be approximated as linear-elastic
432 although some non-linearity is observed in the saturated specimen and attributed to the
433 softening of the matrix. The hysteresis in the unloading curve was found to increase with
434 exposure time.

435

436 The measured torsional shear modulus of the group C and D CFRP tendons exposed in
437 distilled water at either 23°C or 60°C, can be seen in Figure 7. In this figure, the predicted
438 Fickian mass uptake was calculated for each exposure time and plotted. Group C and D
439 have different diffusion coefficient values and therefore have different mass uptake values
440 for the same exposure time. The error bars plotted correspond to one standard deviation
441 representing the variation between the three experimental load runs.

442

443 The dried shear modulus for group D-I is $G_o = 5.91$ GPa, whereas the dried shear modulus
444 for group C-II is $G_o = 5.19$ GPa, which is 12% lower. Groups C and D have the same
445 epoxy, fibre type and fibre volume, so this deviation is attributed primarily to the void
446 content in group C. For both groups the shear modulus decreased with moisture ingress
447 but the reduction was greater for Group C. A 17% decrease in shear modulus for the group
448 D specimens (D-I-9 sample) is observed after 141 days of exposure at 23°C plus 71 days
449 of exposure at 60°C. This exposure regime is equivalent to 1.05% moisture absorption. A
450 drop of around 29% is observed in group C (C-I-8 sample) for the same exposure
451 conditions and exposure time period that corresponds to a higher mass uptake $M_t = 1.77\%$.
452 By defining the shear modulus degradation as G_t/G_o , the results for groups C and D for
453 similar mass uptakes are listed in the Table 2. Even for a given percentage of M_t/M_{sat} ,
454 Group C shows a somewhat greater degradation than group D and again this is attributed
455 to the voids and differences in the production process. Note that for similar mass uptakes
456 the C-I-6 specimen shows a greater degradation than C-II-4 and -5 perhaps due to
457 microcracking in the clamping region with the flat profile clamps. As discussed, this
458 phenomenon was avoided in subsequent tests by changing the clamping system.

459 For the C-II specimens exposed at 60°C the shear modulus appears to reduce gradually at
460 around 3.70 GPa for $M_{sat} = 2.1\%$ and it is deduced there exists a shear modulus at saturation

461 G_{sat} (as illustrated in Figure 10). This phenomenon is attributed to the softening of the
462 matrix material. The shear modulus at the saturation point is not clearly defined in group
463 D-I but it seems to approach $G= 4.94$ GPa for $M_f=1.05\%$. The G_{sat} values will be verified
464 for both groups by testing further a CFRP specimen, when full saturation at 23°C is
465 reached.

466

467 Specimens in the C-II series with the same predicted mass uptakes after exposure at either
468 23°C or 60°C exhibit similar shear moduli values. This consistency generates confidence
469 in the 60°C accelerated ageing process and suggests the higher temperature does not
470 exacerbate any material deterioration. Insignificant changes in shear moduli are observed
471 in the C-II specimens with the same Fickian mass uptakes, regardless of whether that time
472 point represented the first or second time of testing. Consequently, it can be inferred that,
473 within the experimental load range, there is a negligible correlation between any
474 microcracking from repetitive testing and subsequent degradation mechanisms in the
475 epoxy material.

476

477 **Prediction model**

478 Design models have been developed to predict the mechanical degradation behaviour of
479 FRPs due to exposure in wet environments. However, the main focus tends to be on fibre
480 dominated properties. The formulations described here (Papanicolaou et al. 2006; Phani
481 and Bose 1987; Chen et al. 2007b) include an exponential term that potentially reflects the
482 exponential Fickian mass uptake behaviour. The substantive difference between the
483 models lies in the value of the exponential term that represents the rate of mechanical
484 degradation.

485 Phani and Bose (1987) studied E-glass Chopped Strand Mat (CSM) laminates HSR 8131
 486 (Bakelite Hylam Ltd, India) under hygrothermal conditions and showed that the flexural
 487 strength can be expressed as:

$$488 \quad \sigma(t) = (\sigma_0 - \sigma_\infty) \exp(-t / \tau) + \sigma_\infty \quad (3)$$

489 Where $\sigma(t)$ is the flexural strength at exposure time t , σ_0 and σ_∞ are the flexural strength at
 490 zero and infinite time respectively and τ is a time variable that increases with increasing
 491 temperature according to:

$$492 \quad 1 / \tau = 1 / \tau_0 \exp(-E_a / RT) \quad (4)$$

493 where E_a is the activation energy, R is the Universal gas constant and T is the temperature
 494 in Kelvin. Chen et al. (2007b) studied the long-term durability of glass FRP bars in
 495 concrete pore solution and assumed a total loss of the tensile strength at infinite time by
 496 adopting the relationship:

$$497 \quad Y = 100 \exp(-t / \tau) \quad (5)$$

498 where Y is the tensile strength retention (%), t is the exposure time, τ is $1/k$ and k is the
 499 degradation rate. Consequently, the steepness of the exponential curve is a function of the
 500 degradation rate k . However, equation 5 was developed for glass FRP bars with a polyester
 501 matrix where the matrix decomposes under longer exposure times and at higher
 502 temperatures, and the glass fibres leach out. A generic model to describe the mechanical
 503 degradation in different types of unreinforced polymers was proposed by Papanicolaou et
 504 al. (2006) and called the RPM model

$$505 \quad \frac{P_t}{P_0} = s + (1 - s) \exp(-sM_t) \quad (6)$$

506 where P_t represents the mechanical property at exposure time t , M_t is the percentage mass
 507 uptake at exposure time t and $s = P_\infty / P_0$ at the saturation point. The model was applied to

508 epoxy specimens exposed in distilled water at 60°C and 80°C and tested in 3 point bending
509 (Papanicolaou et al. 2006).

510 The RPM model was used to predict the expected shear stiffness at a given time and
511 compared with the experimental findings for groups C and D in Figure 8. The RPM input
512 degradation rates of 0.709 and 0.836 were found using $s = G_{sat}/G_o$ as derived from the latest
513 experimental data for group C and D respectively. The RPM model seems to agree better
514 with the experimental findings of groups C-II series than with group D. However, for both
515 groups the predictions tend to deviate near the saturation point. One issue in this
516 calculation is that the degradation ratio is assumed to be the same throughout the bulk of
517 the tendon. Yet in practice the conditions in a torsion test are not uniform since the
518 moisture diffuses inwards from the outer tendon surface and the torsional contribution of a
519 given annulus depends on the distance from the centre of the tendon.

520
521 To more accurately reflect these details, a predictive model was developed to relate the
522 diffusion process through the cross-section of the CFRP specimens and the shear stiffness
523 degradation mechanism. It is assumed that, as the solution ingress proceeds from the outer
524 tendon surface towards the centre of the cross-section, the shear stiffness of the ‘degraded’
525 regions (outermost regions) is decreased by a certain factor that is dependent on the
526 moisture concentration C . At full saturation a residual stiffness G_{sat} remains. The model is
527 based on the Fickian diffusion process. The solution procedure is as follows:

528 • The tendon radius is discretised to a series of n rings (taken as $n=200$ in the current work)
529 and the concentration profile along the radius is calculated (see Figure 9a). The
530 concentration profile is derived in terms of percentage moisture concentration by
531 assuming that the solution at the tendon surface has a concentration equal to 1.00.

532 • The average concentration value of each ring for the specific time point is calculated as:

$$533 \quad C_{avi} = (C_i + C_{i+1}) / 2 \quad (7)$$

534 and is assumed to be constant over the area of the segment.

535 • The shear stiffness of each ring ΔG_i which is over and above G_{sat} is defined as:

$$536 \quad \Delta G_i = (1 - C_{avi}) \cdot (G_o - G_{sat}) \quad (8)$$

537 where G_o is the shear modulus of the tendon in the dry condition, G_{sat} is the shear
538 modulus of the tendon at saturation and C_{avi} is the average concentration of the segment.

539 The $(G_o - G_{sat})$ component reflects the degradation of the matrix component due to
540 moisture uptake between $t=0$ and $t=\infty$. The $(1 - C_{avi})$ is a degradation factor based on the
541 concentration of the solution and when a region is fully saturated $C_{avi}=1.00$.

542 • The ΔG_i values are integrated across the section according to the polar second moment of
543 area J as derived by the torsion shear stress distribution across the section (Equation
544 9). The polar second moment of area for a cylindrical annulus with an inner radius r_i and
545 outer radius r_{i+1} , is denoted as J_i . When the shear stiffness values of the annuli vary with
546 moisture uptake e.g. equation 8, then the equivalent averaged contribution to the overall
547 tendon shear stiffness ΔG_{eq} above G_{sat} can be defined as:

$$548 \quad \Delta G_{eq} = \frac{\sum_{i=1}^n \Delta G_i J_i}{J} \quad (9)$$

549 where $J_i = \frac{\pi(r_{i+1}^4 - r_i^4)}{2}$ and J is the polar second moment of area of the solid tendon.

550 • The resulting G_t value for the tendon after exposure time t is then:

$$551 \quad G_t = G_{sat} + \frac{\sum_{i=1}^n (1 - C_{avi}) J_i}{J} (G_o - G_{sat}) \quad (\text{see Figure 9b}) \quad (10)$$

552 subject to the following boundary conditions: as $t \rightarrow 0$, $G_t = G_o$ and as $t \rightarrow \infty$, $G_t = G_{sat}$.

553

554 Figure 10 illustrates the comparison between the experimental data and the prediction
555 models for both groups C and D. To plot the shear modulus versus the exposure time it
556 was necessary to use a common baseline for the 23°C and the accelerated 60°C results.
557 The time axis in Figure 10 therefore corresponds to exposure at 23°C and so time shift
558 factors were applied for the specimens exposed at 60°C to convert these readings to
559 equivalent exposure times at 23°C. The time shift factors were calculated as the ratio of
560 mass uptake rate at 60°C to the respective one at 23°C at specific exposure times leading
561 to factors of 12 and 10 for group C and D respectively. The prediction model seems to
562 underpredict the shear modulus values for the initial exposure times up to 141 days for
563 both groups C and D, but generally captures the trend of the experimental findings.

564

565 **Implications and further developments**

566 The full immersion of the CFRP tendons results in direct contact with water whereas in
567 CFRP prestressed concrete the concrete cover will offer a protective casing to the tendons.
568 Hence, the exposure conditions in the current work could be rather onerous compared with
569 what might be expected in practice. A loss of matrix stiffness over time will have
570 implications for matrix-dominated properties such as the bond behaviour of CFRP tendons
571 in concrete. This will be of particular relevance in cases where the outer resin rich layer of
572 the tendon surface is a major contributor to the bond resistance. A study on the long-term
573 durability of bond strength between CFRP tendons and concrete is on-going.

574

575 **Conclusions**

576 The mass uptake and torsional stiffness behaviour over exposure time of two tendon
577 groups C and D with the same material characteristics (epoxy, fibre type, fibre volume) but

578 different production processes were investigated. The Group C tendons were uncoated
579 whereas Group D samples were sand coated and so were subjected to additional curing to
580 affix the sand particles to an outer resin layer. The T_g values measured using DMA tests
581 were inconclusive in terms of identifying differences in the crosslink density between
582 groups C and D. Group C tendons immersed in water exhibited a 60% greater mass uptake
583 at saturation than group D. This was primarily attributed to the presence of voids, as
584 observed in the optical microscope pictures. Torsion test results show that the shear
585 stiffness of the CFRP tendon specimens immersed in distilled water degrades with time.
586 For the group C specimens a 29% decrease in the shear modulus was measured after 325
587 days of exposure at 60°C (C-II series) and by this time the tendons appeared to have
588 reached saturation. For group D the reduction in stiffness was lower, 17%, and this was
589 attributed to the lower moisture uptake rate. However, further testing is required to confirm
590 the group D shear modulus at saturation. The use of 60°C as an accelerated temperature
591 did not appear to induce additional degradation even at longer exposure times. A
592 prediction model that relates the time-dependent radial diffusion through a CFRP tendon
593 and the shear modulus contribution from each segment in a discretised section was
594 proposed. The model generally showed good agreement with the experimental findings for
595 both groups C and D.

596

597 **Acknowledgements**

598 We are grateful to SACAC for their technical and financial support. We also appreciate the
599 financial support from the Onassis Foundation.

600

601 **References**

- 602 Abanilla, M.A, Karbhari, V.M. and Li, Y. (2006). “Interlaminar and intralaminar durability
603 characterization of wet layup carbon/epoxy used in external strengthening.” *Composites Part*
604 *B*, 37(7-8), 650-661.
- 605 ACI 440.1-R06 (2006). Guide for the design and construction of concrete reinforced with FRP
606 bars. American Concrete Institute, Farmington Hills, MI, USA.
- 607 Adamson, M.J. (1980). “Thermal expansion and swelling of cured epoxy resin used in
608 graphite/epoxy composite materials.” *J. Mater. Sci.*, 15(7), 1736-1745.
- 609 Ankara, A., Weisgerber, D. and Vilsmeier, J. (1986). “Effect of post-curing on properties of
610 carbon fibre-epoxy composites.” *Mater. Sci. Technol.*, 2(7), 647-651.
- 611 ASTM. (2008). “Standard test method for shear modulus at room temperature.” ASTM E143-
612 02, West Conshohocken, PA.
- 613 Birger, S., Moshonov, A. and Kenig, S. (1989). “The effects of thermal and hygrothermal
614 ageing on the failure mechanisms of graphite-fabric epoxy composites subjected to flexural
615 loading.” *Composites*, 20(4), 341–348.
- 616 Burgoyne, C. and Balafas, I. (2007). “Why is FRP not a financial success?” *Proc., FRPRCS-*
617 *8: 8th Int. Symp. on FRPs for Reinforced Concrete Structures*, edited by T. Triantafillou,
618 University of Patras, Greece, 16-18 July, 1-10.
- 619 Cavaille, J.Y., Johari, G.P. and Mikolajczak, G. (1987). “Dynamic mechanical properties of
620 structural glass fibre-epoxy composites.” *Polymer*, 28(11), 1841-1846.
- 621 Chen, Y., Davalos, J.F., Ray, I. and Kim, H.Y. (2007a). “Accelerated Aging Tests for
622 Evaluations of Durability Performance of FRP Reinforcing Bars for Concrete Structures.”
623 *Compos. Struct.*, 78(1), 101-111.

624 Chen, Y., Davalos, J.F. and Ray, I. (2007b). "Durability prediction for GFRP reinforcing bars
625 using short-term data of accelerated aging tests." *J. Compos. Constr.*, 10(4), 279-286.

626 Crank, J. (1975). *The mathematics of diffusion*. Clarendon Press, Oxford, UK.

627 Davalos, J.F, Chen, Y. and Ray, I. (2008). "Effect of FRP bar degradation on interface bond
628 with high strength concrete." *Cement and Concrete Composites*, 30(8), 722-730.

629 Davies, P., Pomies, F. and Carlsson, L.A. (1996). "Influence of water and accelerated aging on
630 the shear fracture properties of glass/epoxy composite." *Appl. Compos. Mater.*, 3(2), 71-87.

631 Diamant, Y., Marom, G. and Broutman, L. (1981). "The effect of network structure on
632 moisture absorption of epoxy resins." *J. Appl. Polym. Sci.*, 26(9), 3015-3025.

633 Dolan, C.W., Ahearn, E.B, Deng, J., Tanner, J.E. and Mukai, D. (2008). "Durability and
634 accelerated ageing testing of CFRP repair systems." *Proc., CICE 2008: 4th International
635 Conference on FRP Composite in Civil Engineering*, edited by Masoud Motavalli, Zürich,
636 Switzerland, 22-24 July, 22-24.

637 Hancox, N.L. (1972). "The use of a torsion machine to measure the shear strength and
638 modulus of unidirectional carbon fibre reinforced plastics." *Mater. Sci.*, 7(9), 1030-1036.

639 Hancox, N.L. (1977). "The effects of flaws and voids on the shear properties of CFRP." *J.
640 Mater. Sci.*, 12(5), 884-892.

641 Hartt, W. H. and Venugopalan, S. (2002). "Corrosion evaluation of post-tensioned tendons on
642 the Mid Bay Bridge in Destin, Florida." *Florida Department of Transportation Research
643 Center report 33890*.

644 Hiermer, T., Schmitt-Thomas, Kh.G. and Yang, Z.G. (1998). "Mechanical properties and
645 failure behaviour of cylindrical CFRP-implant-rods under torsion load." *Composites Part A*,
646 29(11), 1453-1461.

647 Huang, H. and Talreja, R. (2005). "Effects of void geometry in elastic properties of
648 unidirectional fiber reinforced composites." *Compos. Sci. Technol.*, 65(13), 1964-1981.

649 Huang, J. and Aboutaha, R. (2010). "Environmental reduction factors for GFRP bars used as
650 concrete reinforcement: New Scientific Approach." *J. Compo. Constr.*, 14(5), 479-486.

651 Kelly, A. (1989). "Thermosetting Resin Matrices." *Concise encyclopedia of composite*
652 *materials*, The Pergamon Press, Oxford, UK, 267.

653 Krishna, R., Revathi, A., Srihari, S. and Rao, R. (2010). "Post-curing effects on hygrothermal
654 behavior of RT-cured glass/epoxy composites." *J. Reinf. Plast. Compos.*, 29(3), 325-330.

655 Lam, Y.C., Li, J. and Joshi, S.C. (2003). "Simultaneous optimisation of die-heating and pull-
656 speed in pultrusion of thermosetting composites." *Polym. Compos.*, 24(1), 199-209.

657 Li, S., Ding, Z., Xu, L., Lee, L.J. and Engelen, H. (2002). "Influence of heat transfer and curing
658 on the quality of pultruded composites. I: Experimental." *Polym. Compos.*, 23(5), 947-956.

659 Liu, L., Zhang, B.M., Wang, D.F. and Wu, Z.J. (2006). "Effects of cure cycles on void content
660 and mechanical properties of composite laminates." *Compos. Struct.*, 73(3), 303-309.

661 Lynch, D. (2012). "Hammersmith flyover: returning to full strength" *New Civil Engineer*, 98,
662 14-16.

663 Marais, S., Metayer, M., Nguyen, T.Q., Labbe, M. and Saiter, J.M. (2000). "Diffusion and
664 permeation of water through unsaturated polyester resins-influence of resin curing." *Eur.*
665 *Polym. J.*, 36(3), 453-462.

666 Mayer, R.M. (1996). "Manufacturing considerations." *Design with reinforced plastics*, Bourne
667 Press, London, UK, 136-138.

668 Meyer, F., Sanz, G., Eceiza, A., Mondragon, I. and Mijovic, J. (1995). "The effect of
669 stoichiometry and thermal history during cure on structure and properties of epoxy
670 networks." *Polymer*, 36(7), 1407-1414.

671 Micelli, F. and Nanni, A. (2001). "Issues related to durability of FRP reinforcement for RC
672 structures exposed to accelerated ageing." *Proc., ASC 16th Annual Technical Conference*

673 (CD-ROM), edited by M.W. Hyer and A.C. Loos, Virginia Tech. University, Blacksburg,
674 VA, 9-12 September, 12pp.

675 Min, B.G., Hodgkin, J.H. and Stachurski, Z.H. (1993). "The dependence of fracture properties
676 on cure temperature in a DGEBA/DDS epoxy system." *J. Appl. Polym. Sci.*, 48 (7), 1303-
677 1312.

678 Ogasawara, T., Yokozeki, T., Onta, K. and Ogihara, S. (2007). "Linear and nonlinear torsional
679 behavior of unidirectional CFRP and GFRP." *Compos. Sci. Technol.*, 67(15-16), 3457-3464.

680 Olivier, P., Cottu, J.P. and Ferret, B. (1995). "Effects of cure cycle pressure and voids on some
681 mechanical properties of carbon/epoxy laminates." *Composites*, 26(7), 509-515.

682 Papanicolaou, G.C., Kosmidou, Th.V., Vatalis, A.S. and Delides, C.G. (2006). "Water
683 absorption mechanism and some anomalous effects on the mechanical and viscoelastic
684 behavior of an epoxy system." *J. Appl. Polym. Sci.*, 99(4), 1328-1339.

685 Phani, K.K. and Bose, N.R. (1987). "Temperature dependence of hydrothermal ageing of
686 CSM-laminate during water immersion." *Compos. Sci. Technol.*, 29(2), 79-87.

687 Robert, M., Wang, P., Cousin, P. and Benmokrane, B. (2010). "Temperature as an accelerating
688 factor for long-term durability testing of FRPs: Should there be any limitations?" *J. Compos.*
689 *Constr.*, 14(4), 361-367.

690 Scott P. and Lees J.M. (2012). "Effect of solution exposure on the combined axial-shear
691 behaviour of unidirectional CFRP rods." *Composites Part A*, 43(9), 1599-1611.

692 Vanlandingham, M.R., Eduljee, R.F. and Gillespie, J.W. (1999a). "Relationships between
693 stoichiometry, microstructure, and properties for amine-cured epoxies." *J. Appl. Polym. Sci.*,
694 71(5), 699-712

695 Vanlandingham, M.R., Eduljee, R.F. and Gillespie, J.W. (1999b). "Moisture diffusion in
696 epoxy systems." *J. Appl. Polym. Sci.*, 71(5), 787-798.

697 Wright, W. W. (1981). "The effect of diffusion of water into epoxy resins and their carbon-
698 fibre reinforced composites." *Composites*, 12(3), 201-205.

699 Wu, C.S. (1992). "Influence of post-curing and temperature effects on bulk density, glass
700 transition and stress-strain behaviour of imidazole-cured epoxy network." *J. Mater. Sci.*,
701 27(11), 2952–2959.

702 Xiao, G.Z and Shanahan, M.E.R. (1997). "Water absorption and desorption in an epoxy resin."
703 *J. Polym. Sci.*, 35(16), 2659-2670.

704 Zhu, H., Li, D., Zhang, D., Wu, B. and Chen, Y. (2009). "Influence of voids on interlaminar
705 shear strength of carbon/epoxy fabric laminates." *Trans. Nonferrous Met. Soc. China*, 19(2),
706 s470-s475.

707

708

709

710

711

712

713

714

715

716

717

718

719

720

721

722 **Table 1:** Exposure programme for C-I and C-II series and D-I-series immersed in distilled
 723 water.

Specimen	Exposure temperature (°C)	Exposure time (days)																	
		0	3	7	14	17	27	31	35	63	89	99	104	112	132	141	159	212	325
D-I-6	23				x ^a				x ^a		x								
D-I-7	Dry	x																	
D-I-9	23/60												x		x	x	x		
C-I-6	23				x ^a				x ^a					x ^b					
C-I-8	23/60														x		x	x	
C-I-9	23													x					
C-II-3	Dry	x																	
C-II-4	23			x			x												
C-II-5	23						x			x									
C-II-6	23									x					x				
C-II-7	23														x				
C-II-8	60		x																
C-II-9	60				x	x													
C-II-10	60					x			x										
C-II-11	60								x										x
C-II-12	60								x										x

724 The specimen identification a-b-c denotes a= specimen group C or D; b= experimental
 725 series I or II; c= specimen number; x= time of testing; shaded area=exposure at 60°C.

726 ^a Slightly different torsion test set up

727 ^b Signs of damage at the clamping area

728

729

730

731

732 **Table2:** Shear modulus degradation for similar mass uptake ratios: Comparison between
733 group C and D.

734

Specimen	M_t (%)	M_t / M_{sat}	G_t / G_0
C-II-4	0.389	19%	0.96
C-II-5	0.389	19%	0.96
C-I-6	0.440	21%	0.80
D-I-6	0.266	20%	0.99
C-I-8	1.246	59%	0.75
D-I-9	0.729	56%	0.85

Peer reviewed version

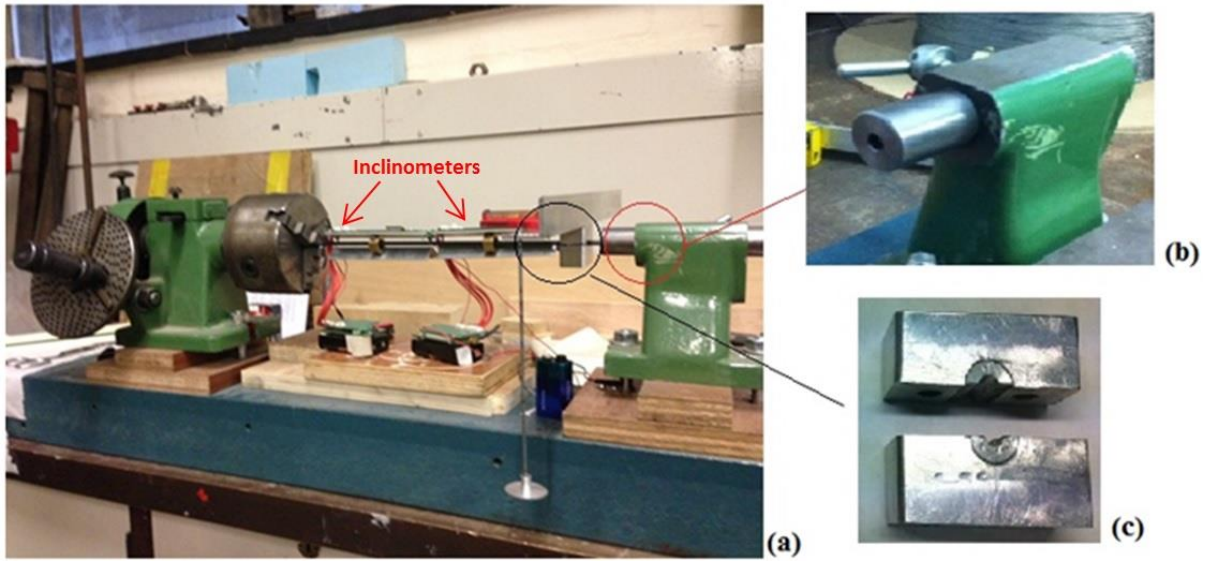


Figure 1. (a) Torsion test set up, b) Axially unrestrained edge and c) Curved clamp.

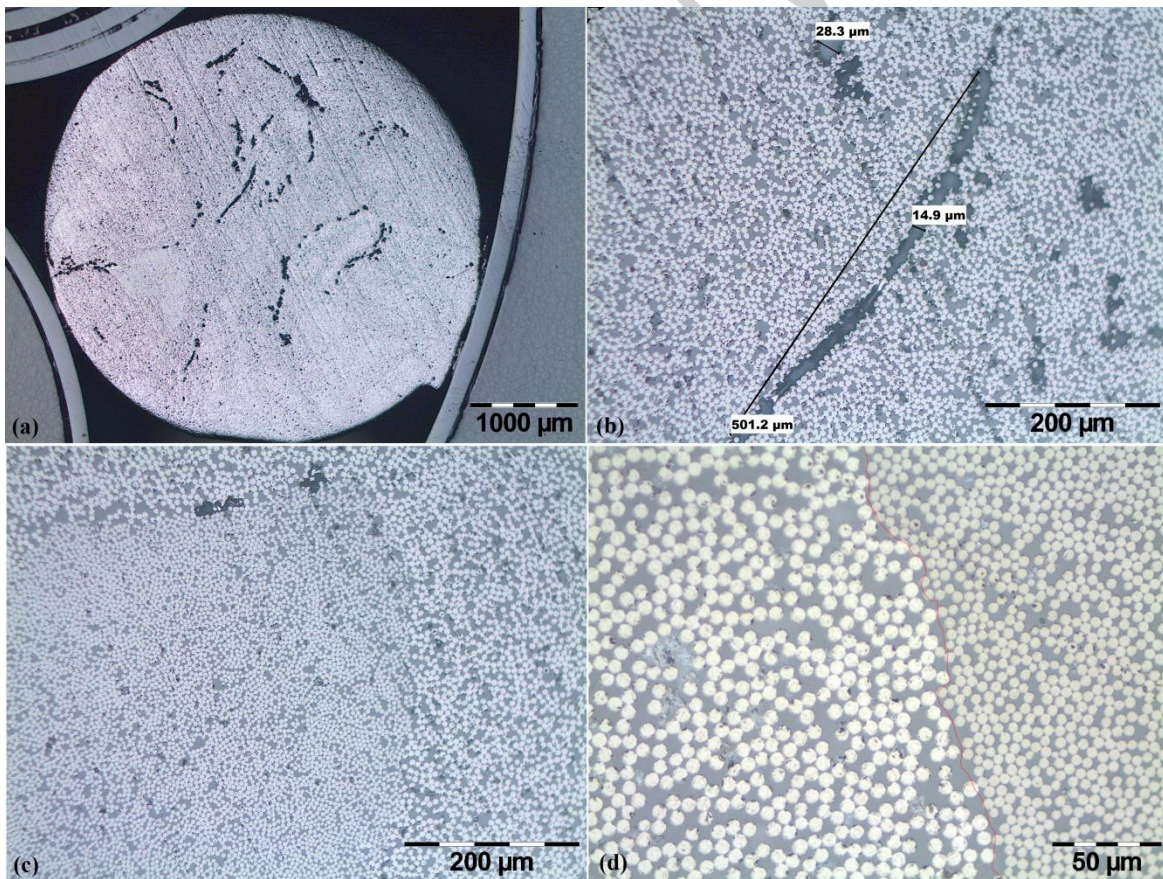


Figure 2. Optical Microscopy: Group C a) 1000 μm , b) void area 200 μm , c) 200 μm interfacial region, d) 50 μm interfacial region.

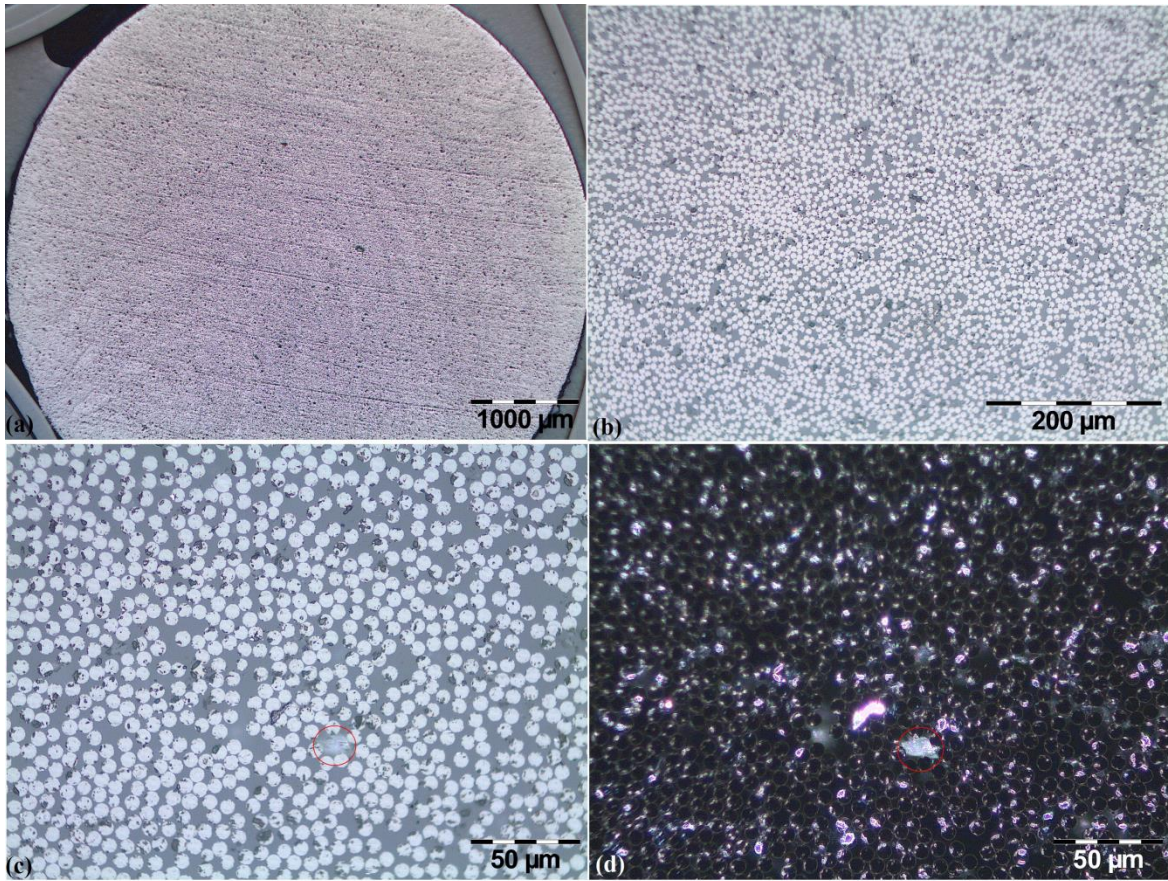


Figure 3. Optical microscopy: Group D a) 1000μm, b) 200 μm, c) 50μm light field and d) 50 μm dark field.

Peer review

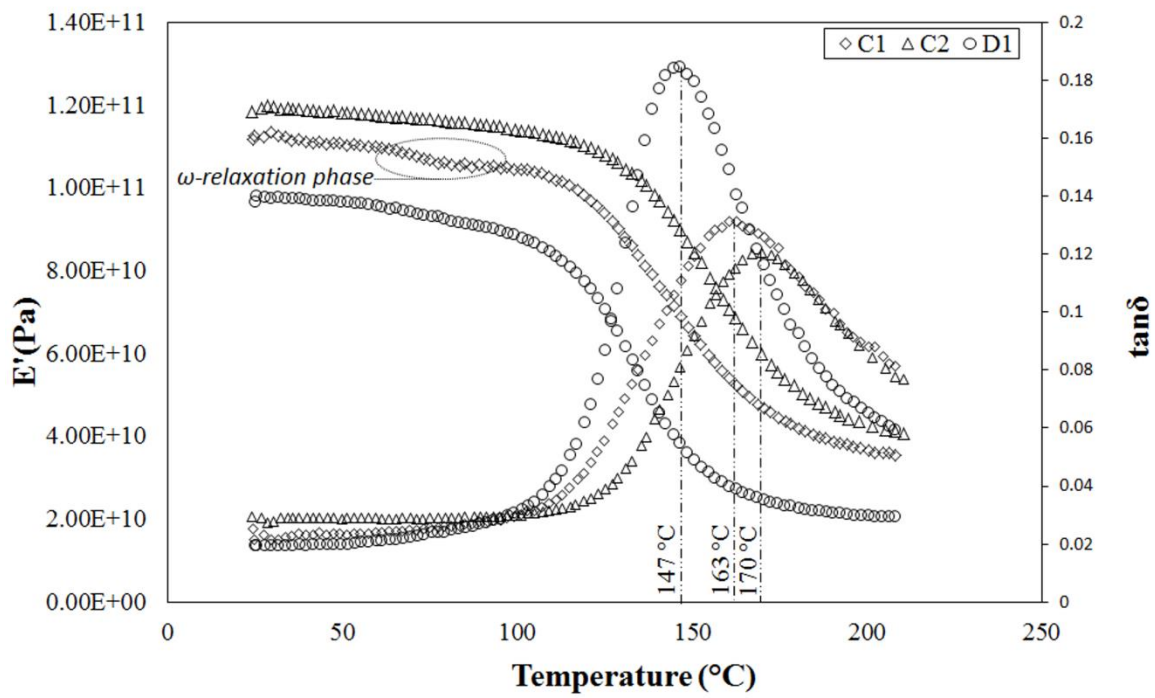


Figure 4. DMA tests group C versus group D.

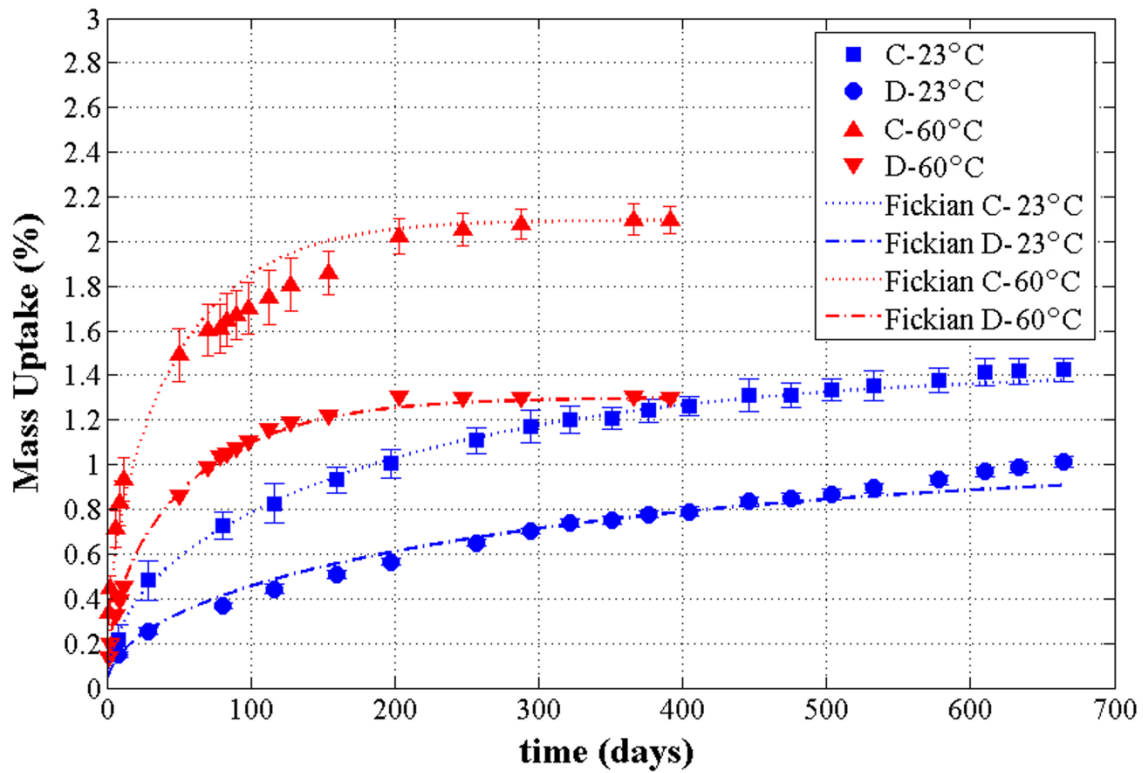


Figure 5. Moisture Uptake in group C and D.

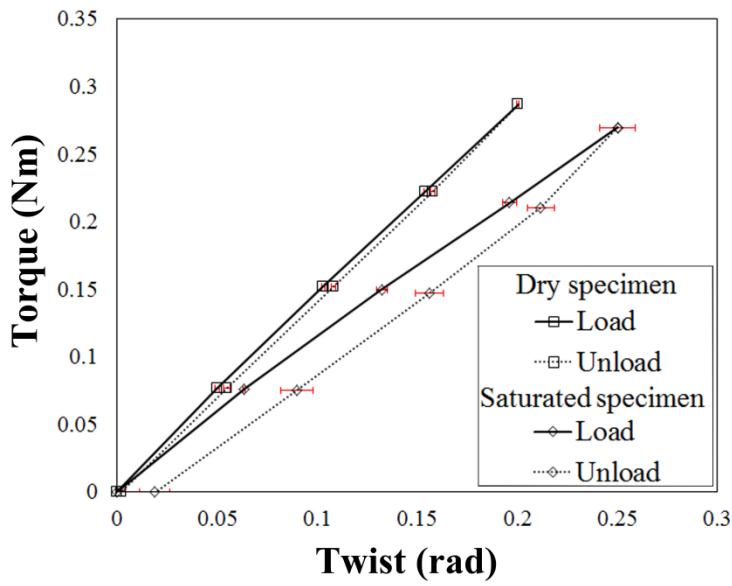


Figure 6. Load-Unload curves for a “dry” specimen, C-II-3, and a “saturated specimen”, C-II-12.

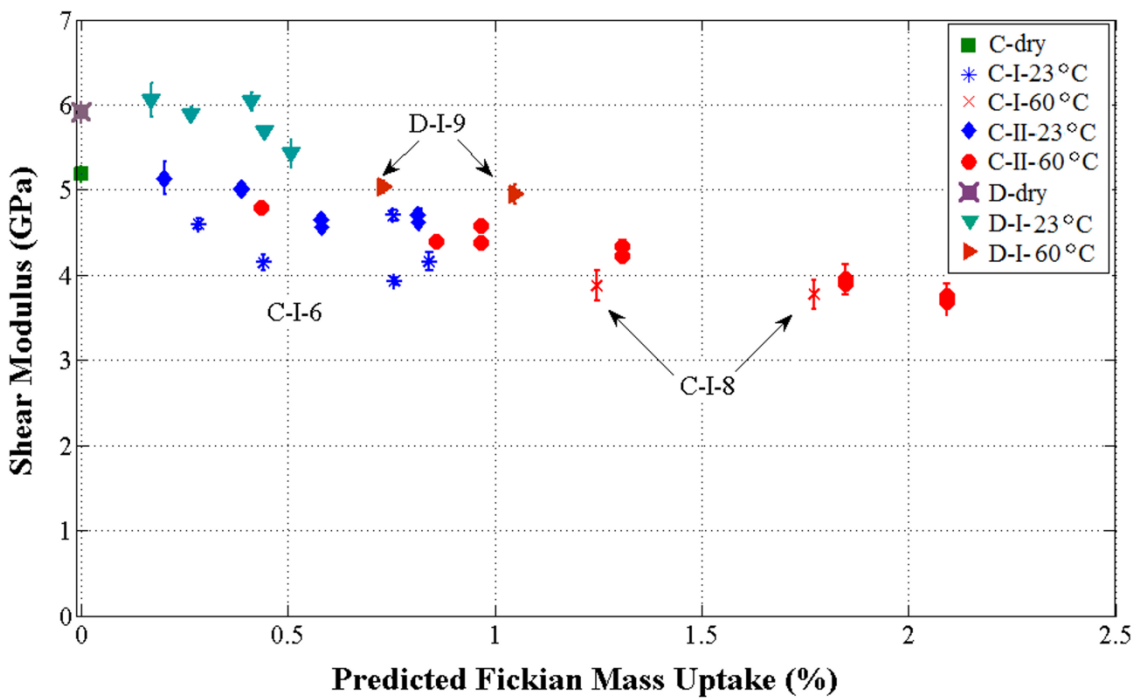


Figure 7. Shear Modulus Degradation with predicted Fickian Mass Uptake: Groups C and D at 23°C and 60°C.

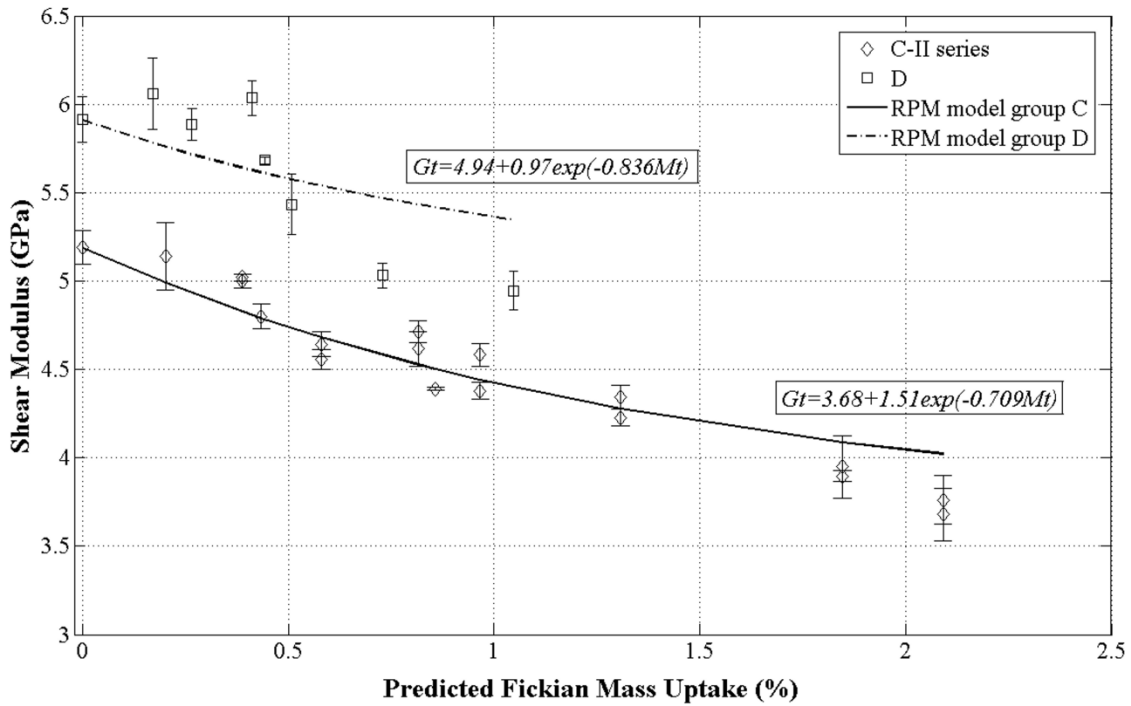


Figure 8. Comparison of RPM model with experimental findings for group C-II and D-I series.

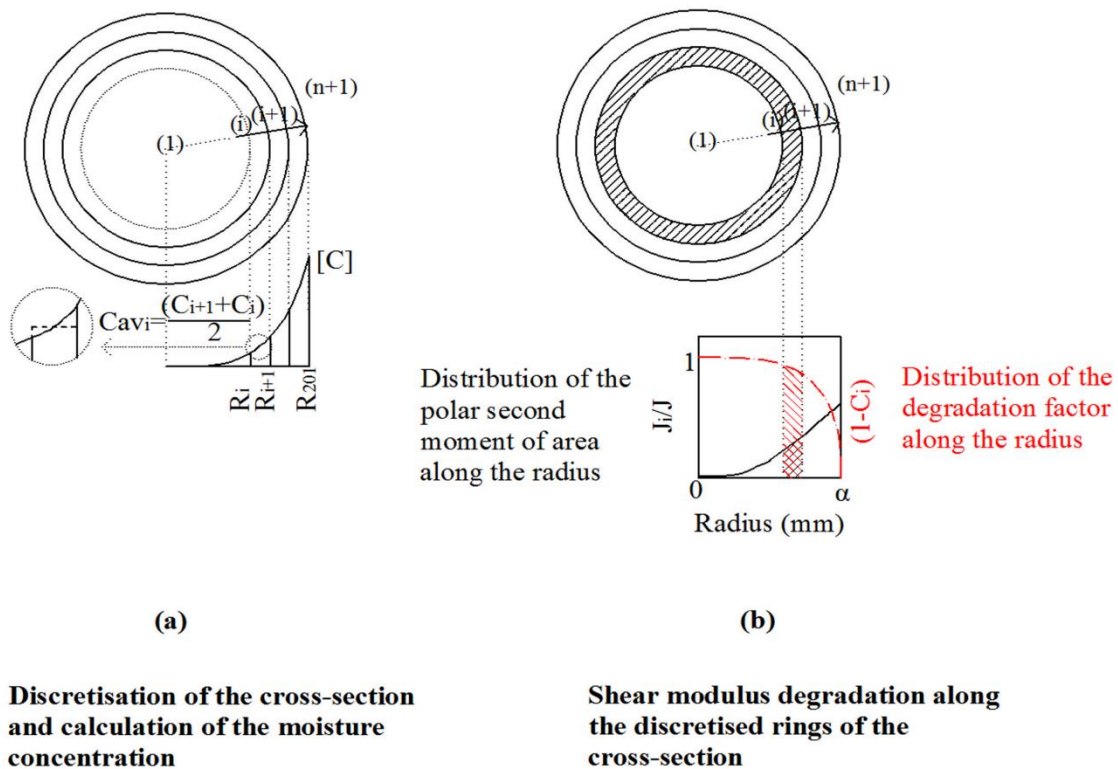


Figure 9. (a) Discretisation of a CFRP tendon section and calculation of the average moisture concentration for each segment, (b) Calculation of the polar second moment of area factor and of the degradation factor for each segment.

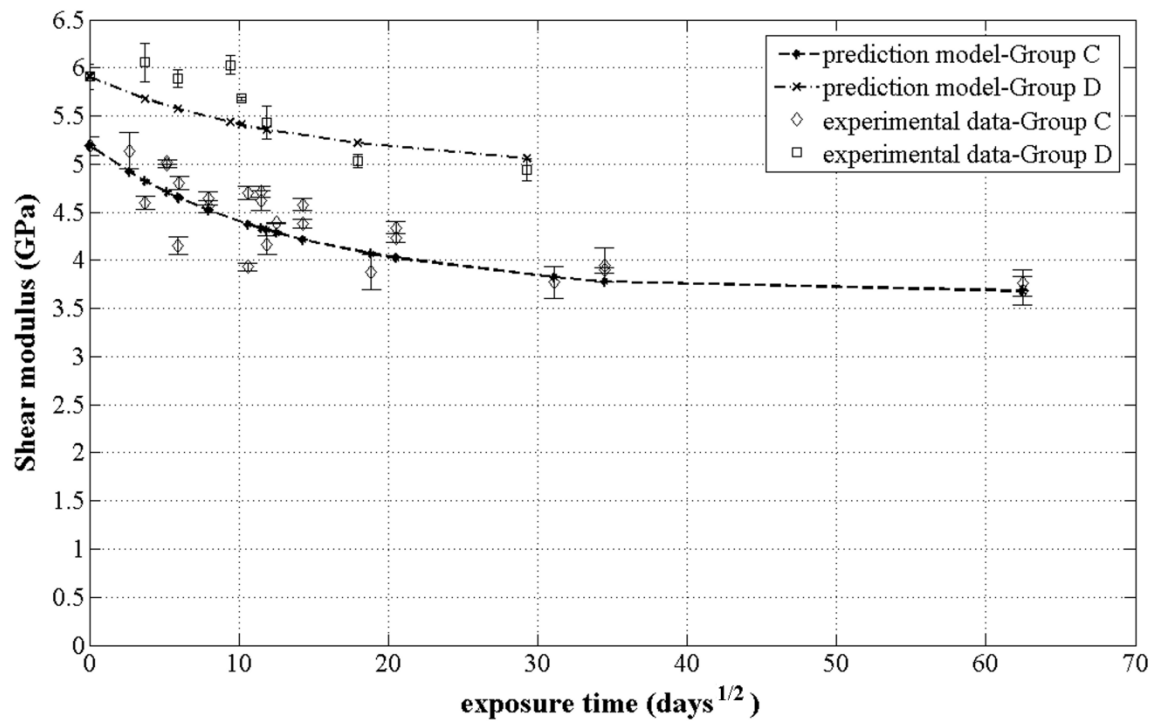


Figure 10. Comparison between the prediction model and the experimental data for groups C-I & II and D-I series.

Peer reviewed